


SWIFT J1749.4-2807

A. Sanna,¹  ^{2,3}

¹*Dipartimento di Fisica, Università degli Studi di Cagliari, SP Monserrato-Sestu km 0.7, 09042 Monserrato, Italy*

²

³

Accepted XXX. Received YYY; in original form ZZZ

ABSTRACT

It should be a single paragraph not more than 250 words (200 words for Letters).

Key words: binaries:general–stars:neutron – X-rays:binaries – accretion: accretion disks

1 INTRODUCTION

2 OBSERVATIONS AND DATA REDUCTION

Normally the next section describes the techniques the authors used. It is frequently split into subsections, such as Section ?? below.

2.1 NICER

NICER (Gendreau et al. 2012) started observing the X-ray transient SWIFT J1749.4-2807 on 2021 March 1 (MJD 59274.6) up to 2021 March 28 (MJD 59301.8) for a total exposure time of almost 141 ks. We processed the NICER observations with the NICERDAS pipeline version 7.0 (version V007a) retaining events in the 0.2–12 keV energy range, for which the pointing offset was <54 arcsec, the dark Earth limb angle was > 30°, the bright Earth limb angle was > 40°, and the ISS location was outside of the South Atlantic Anomaly (SAA). Moreover, we selected events from 52 out of the available 56 aligned pairs of X-ray concentrator optics and silicon drift detectors (Check with Keith).

2.2 XMM-Newton

XMM-Newton (Jansen et al. 2001) triggered a target of opportunity observation of SWIFT J1749.4-2807 (Obs. ID. 0872392001) starting from 2021 March 4 at 08:41 UTC and ending on 2021 March 4 at 16:17 UTC, for a total duration of 56.7 ks. The instrumental set-up during the observation included the Epic-pn (PN) camera operated in timing mode, the Epic-MOS 1–2 in small window and timing mode, respectively, while the RGS in spectroscopy mode. For the purpose of this work we focused on the PN observation only. We extracted the PN dataset using the Science Analysis Software (SAS) v.19 with up-to-date calibration files. We retained events in the energy range 0.5–10 keV, by selecting optimally calibrated events with PATTERN ≤ 4 and (FLAG = 0). We filtered source and background events from the PN instrument within the RAWX regions [29:47] and [2:8], respectively. We investigated for possible high background flaring activity by constructing a 20s resolution light-curve of the source event at energies larger than 10 keV, but we found none. The 0.5–10

keV light-curve of the source shows an average count-rate around 40 counts per seconds. Superimposed are clearly visible six type-I X-ray bursts almost evenly spaced with a recurrence time of 2.2 hours, and two full X-ray eclipses.

2.3 NuSTAR

2.4 Timing analysis

Both NICER and XMM-Newton observations registered several X-ray type-I bursts and X-ray eclipses during the outburst of the source. To investigate the temporal behaviour of the X-ray pulsar we decided to exclude them from the analysis by ignoring time intervals of ±50 seconds before and after the events. Moreover, we retained only events with energies within the range 0.5 to 10 keV. We then corrected the photon arrival times to the solar system barycenter using the Chandra coordinates of the source (Jonker et al. 2013).

Starting from the timing solution obtained for the first outburst of the source (Markwardt & Strohmayer 2010), we applied barycentric correction to the photon time of arrivals of the NICER and XMM-Newton datasets to account for the Doppler effect in the binary system assuming a circular orbit (see e.g. Burderi et al. 2007; Sanna et al. 2016, for a detailed description of the method). Following on the preliminary detection of the X-ray pulsation during the 2021 outburst of the source (Bult et al. 2021), we updated the time of passage from the ascending node (T_{ASC}) to be able to recover the coherent signal. Before applying phase coherent timing analysis, we refined the values of the local T_{ASC} and the mean spin frequency. We explored the local T_{ASC} value by sampling the interval $59274.49427 \pm P_{orb}/2$ at 1 second steps. For each T_{ASC} value we corrected the applied barycentric correction keeping the other orbital parameters fixed. We then applied epoch-folding searching techniques of the whole dataset using 16 phase bins by exploring the frequency space around the value reported by Bult et al. (2021) with steps of 10^{-8} Hz for a total of 10001 steps. Under the assumption that the best orbital solution is represented by the folded pulse profile at largest χ^2 value in the epoch-folding search (see e.g. Kirsch et al. 2004), we obtained $T_{ASC} = 59274.49428$ MJD and $\bar{\nu} = 517.92001388$. It is worth noting that the estimated local T_{ASC} value significantly differs from the predicted value obtained by propagating the orbital solution reported by (Markwardt & Strohmayer 2010) assuming a constant orbital

* E-mail: andrea.sanna@dsf.unica.it

period. As it will be discussed in detail in the next sections, the latter result suggests the presence of a significant evolution of the orbital period of the system.

To perform coherent timing analysis, we applied the updated local timing solution to create 8-phase-bin pulse profiles by epoch-folding 2000 s-long data segments at the mean spin frequency $\bar{\nu}$. If required, we adjusted the length of the data segments in order to improve the significance of the pulse profiles. We modelled the pulse profiles by fitting a constant plus a superposition of two harmonically related sinusoidal components. We retained only harmonics for which the ratio between the sinusoidal amplitude and the corresponding 1σ uncertainty is equal or greater than three. For each significant component we inferred the fractional amplitude defined as the ratio between the sinusoidal amplitude and the source photons collected to create the pulse profile (i.e. total number of photons in the profile minus the corresponding background) and the fractional part of the phase residual. Higher harmonics were not required to describe the pulse profile.

The second panel of Fig. 1 shows the evolution of the background corrected fractional amplitude of the fundamental (solid squares) and second harmonic (empty circles) components of the NICER (black points) and XMM-Newton (red points) datasets during the outburst. Upper limits (triangles) at 3σ confidence level are reported for the time intervals in which no significant detection was available.

We modelled the fundamental and second harmonic components describing the pulse profiles of the source by applying standard timing techniques (see e.g. Burderi et al. 2007; Sanna et al. 2018, for more details). More specifically, we modelled the phase temporal evolution as:

$$\Delta\phi(t) = \phi_0 - \Delta\nu_0(t - T_0) - \frac{1}{2}\dot{\nu}(t - T_0)^2 + R_{orb}(t), \quad (1)$$

whith ϕ_0 , $\Delta\nu_0$ and $\dot{\nu}$ representing a constant phase, the correction factor on the frequency used to epoch-fold the data, and the spin frequency derivative referred to the epoch T_0 . $R_{orb}(t)$ describes the residual orbital modulation arising from differential corrections between the guessed NS ephemeris and the real one (see e.g. Deeter et al. 1981).

We iteratively repeated this process for each refined ephemeris until no significant improvements were found for any of the model parameters. In Table ?? we list the the orbital best-fit parameters as well as the spin frequency parameters obtained independently from the analysis of the fundamental and second harmonic components. In the third and fourth pannels of Fig. 1 we show the phase delay residuals with the best-fitting models for the fundamental and second harmonic, respectively.

To take into account the values of $\chi^2 > 1$, we rescaled the uncertainties on the parameters reported in Tab. 1 by a factor $\sqrt{\chi^2}$ (see e.g. Finger et al. 1999).

We investigated the contribution of the positional uncertainties on the spin frequency and its derivative by considering the residuals induced by the Earth's motion assuming small variations of the source position $\delta\lambda$ and $\delta\gamma$ (ecliptic coordinates) expressed by the relation:

$$R_{pos}(t) = -\nu_0 y [\sin(M_0 + \epsilon) \cos \gamma \delta\lambda - \cos(M_0 + \epsilon) \sin \gamma \delta\gamma], \quad (2)$$

where $y = r_E/c$ represents the Earth semi-major axis in light-seconds, $M_0 = 2\pi(T_0 - T_v)/P_\oplus - \lambda$, T_v and P_\oplus are the vernal point and the Earth orbital period, respectively, and $\epsilon = 2\pi(t - T_0)/P_\oplus$ (see, e.g. Lyne & Graham-Smith 1990). Given the short duration of the outburst with respect to Earth's orbital period, we can solve Eq. 2 by expanding it in series of $\epsilon \ll 1$ (see e.g. Burderi et al. 2007, and references therein). This allows to estimate upper limits on the spin

frequency correction and the spin derivative as $\sigma_{\nu_{pos}} \leq \nu_0 y \sigma_\nu (1 + \sin^2 \gamma)^{1/2} 2\pi/P_\oplus$ and $\sigma_{\dot{\nu}_{pos}} \leq \nu_0 y \sigma_\nu (1 + \sin^2 \gamma)^{1/2} (2\pi/P_\oplus)^2$, respectively, where σ_ν represents the positional error circle. Using the source position reported in Tab. 1 (Jonker et al. 2013), we estimated $\sigma_{\nu_{pos}} \leq 1.4 \times 10^{-7}$ Hz and $\sigma_{\dot{\nu}_{pos}} \leq 3 \times 10^{-14}$ Hz/s, respectively. We added in quadrature these systematic uncertainties to the statistical errors of ν_0 and $\dot{\nu}$ estimated from the timing analysis.

The average pulse profile differs significantly from a sinusoidal function. It is well described by using a combination of two sinusoids shifted in phase. The XMM-Newton (NuSTAR) fundamental and second harmonic have background-corrected fractional amplitudes of 5.6% (4%) and 3.4% (1.6%), respectively. For the NICER average profile we obtain fractional amplitudes of 4.7% and 3.1% for the fundamental and second harmonic (not corrected for the background), respectively.

3 RESULTS

4 DISCUSSION

The last numbered section should briefly summarise what has been done, and describe the final conclusions which the authors draw from their work.

ACKNOWLEDGEMENTS

REFERENCES

- Bult P. M., et al., 2021, The Astronomer's Telegram, **14428**, 1
- Burderi L., et al., 2007, *ApJ*, **657**, 961
- Deeter J. E., Boynton P. E., Pravdo S. H., 1981, *ApJ*, **247**, 1003
- Finger M. H., Bildsten L., Chakrabarty D., Prince T. A., Scott D. M., Wilson C. A., Wilson R. B., Zhang S. N., 1999, *ApJ*, **517**, 449
- Gendreau K. C., Arzoumanian Z., Okajima T., 2012, in Takahashi T., Murray S. S., den Herder J.-W. A., eds, Society of Photo-Optical Instrumentation Engineers (SPIE) Conference Series Vol. 8443, Space Telescopes and Instrumentation 2012: Ultraviolet to Gamma Ray. p. 844313, doi:10.1117/12.926396
- Jansen F., et al., 2001, *A&A*, **365**, L1
- Jonker P. G., Torres M. A. P., Steeghs D., Chakrabarty D., 2013, *MNRAS*, **429**, 523
- Kirsch M. G. F., Mukerjee K., Breittellner M. G., Djavidnia S., Freyberg M. J., Kendziorra E., Smith M. J. S., 2004, *A&A*, **423**, L9
- Lyne A. G., Graham-Smith F., 1990, Pulsar astronomy. Cambridge University Press
- Markwardt C. B., Strohmayer T. E., 2010, *ApJ*, **717**, L149
- Sanna A., et al., 2016, *MNRAS*, **459**, 1340
- Sanna A., et al., 2018, *A&A*, **617**, L8

This paper has been typeset from a \LaTeX file prepared by the author.

Parameters	Fundamental	Second Harmonic
R.A. (J2000)	$17^h 49^m 31^s.73 \pm 0.6^s$	
Decl. (J2000)	$-28^\circ 08' 05''.08 \pm 0.6''$	
Orbital period P_{orb} (s)	31740.84(1)	31740.8417(27)
Projected semi-major axis $a \sin i/c$ (lt-s)	1.89956(3)	1.899568(11)
Ascending node passage T_{NOD} (MJD)	59274.494176(5)	59274.4941787(14)
Eccentricity (e)	$3.7(3.3) \times 10^{-5}$	$4.1(1.1) \times 10^{-5}$
$\chi^2/\text{d.o.f.}$	1001.6/84	97.8/60
Spin frequency ν_0 (Hz)	517.92001572(25)*	517.92001385(16)*
Spin frequency 1st derivative $\dot{\nu}_0$ (Hz/s)	$-4.0(5) \times 10^{-12}$ *	$-0.6(1.1) \times 10^{-13}$ *

Table 1. Timing solution obtained from the analysis of the NICER and XMM-Newton observations collected during the whole 2021 outburst of SWIFT J1749.4-2807. The orbital solution is referred to the epoch $T_0=59274.6$ MJD. Errors are at 1σ confidence level.* Uncertainties have been calculated including the contribution of the positional uncertainties.

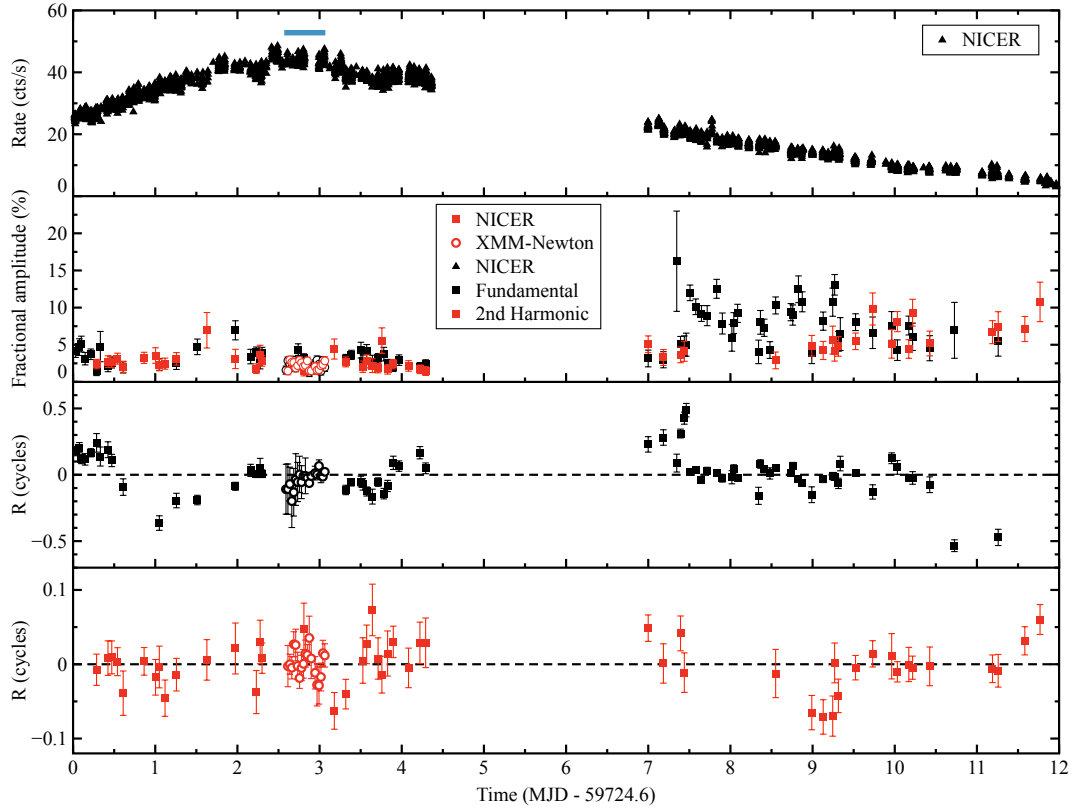


Figure 1. *First panel* - NICER 0.5-10 keV light-curve of the 2021 outburst of the accreting millisecond X-ray pulsar SWIFT J1749.4-2807. The blue segment identifies the time interval in which the XMM-Newton observation has been performed. *Second panel* - Time evolution of the fractional amplitude determined for the fundamental (black points) and the second harmonic (red points) components used to model the source pulse profiles created from the NICER (filled squares) and XMM-Newton (empty circles) datasets. *Third panel* - Fundamental pulse phase residuals in units of phase cycles relative to the best-fitting solution. *Fourth panel* - Second harmonic pulse phase residuals in units of phase cycles relative to the best-fitting solution.